Distribution and sources of organic matter in submarine canyons incising the Gulf of Palermo, Sicily

Sarah Paradis[1], Hannah Gies[2], Davide Moccia[3], Julie Lattaud[4], Lisa Bröder[2], Negar Haghipour[2,5], Antonio Pusceddu[3], Albert Palanques[6], Pere Puig[6], Claudio Lo Iacono[6], Timothy I. Eglinton[2]

[1]Environmental Physics, Institute of Biogeochemistry and Pollutant Dynamics, ETH Zurich, Zürich, Switzerland
[2]Geological Institute, ETH Zürich, Switzerland
[3]Dipartimento di Scienze della Vita e dell'Ambiente, Università degli Studi di Cagliari, Cagliari, 09126, Italy
[4]Environmental Science department, Stockholm University, 11418 Sweden
[5]Laboratory for Ion Beam Physics, Department of Physics, ETH Zürich, 8093 Zürich, Switzerland
[6]Marine Sciences Institute, Consejo Superior de Investigaciones Científicas, Barcelona, 08003, Spain

Correspondence to: Sarah Paradis (sparadis@ethz.ch)

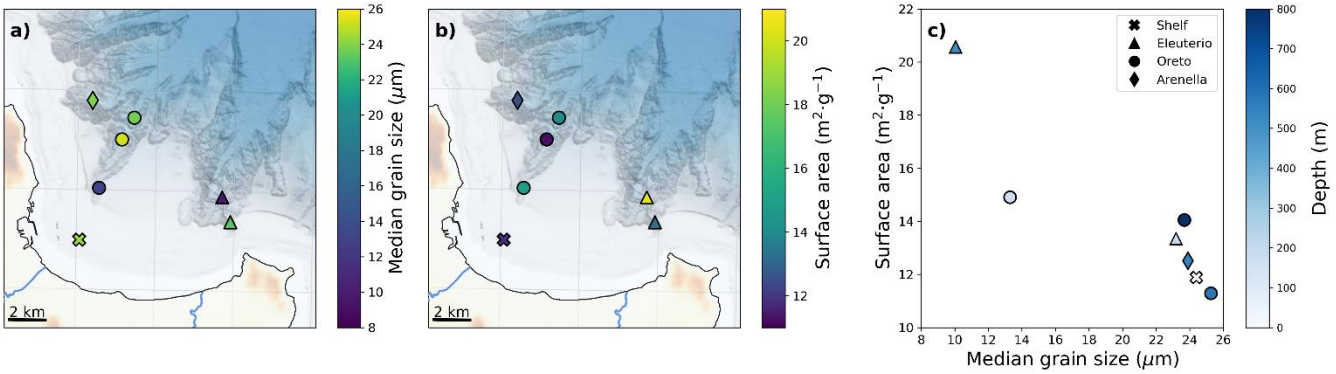

Figure S1. Spatial distribution of a) median grain size and b) mineral surface area. c) Relationship between median grain size and mineral surface area. Colour bars are adjusted to highlight the minimum, mean, and maximum values for each variable.

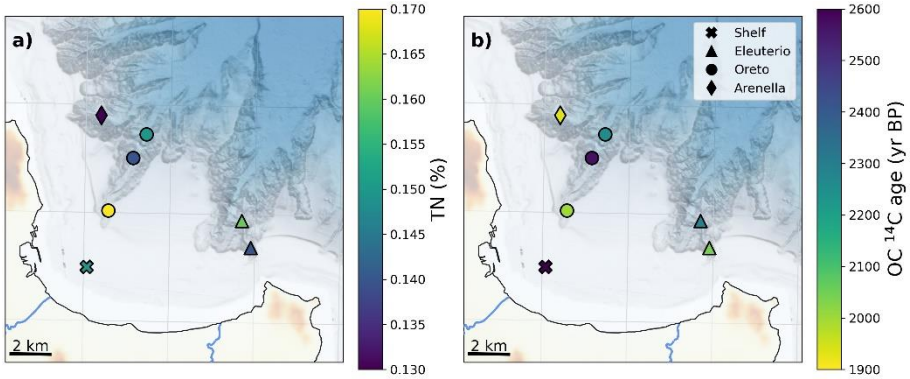

Figure S2. Spatial distribution of bulk parameters: a) TN, b) radiocarbon age. Colour bars are adjusted to highlight the minimum, mean, and maximum values for each variable.

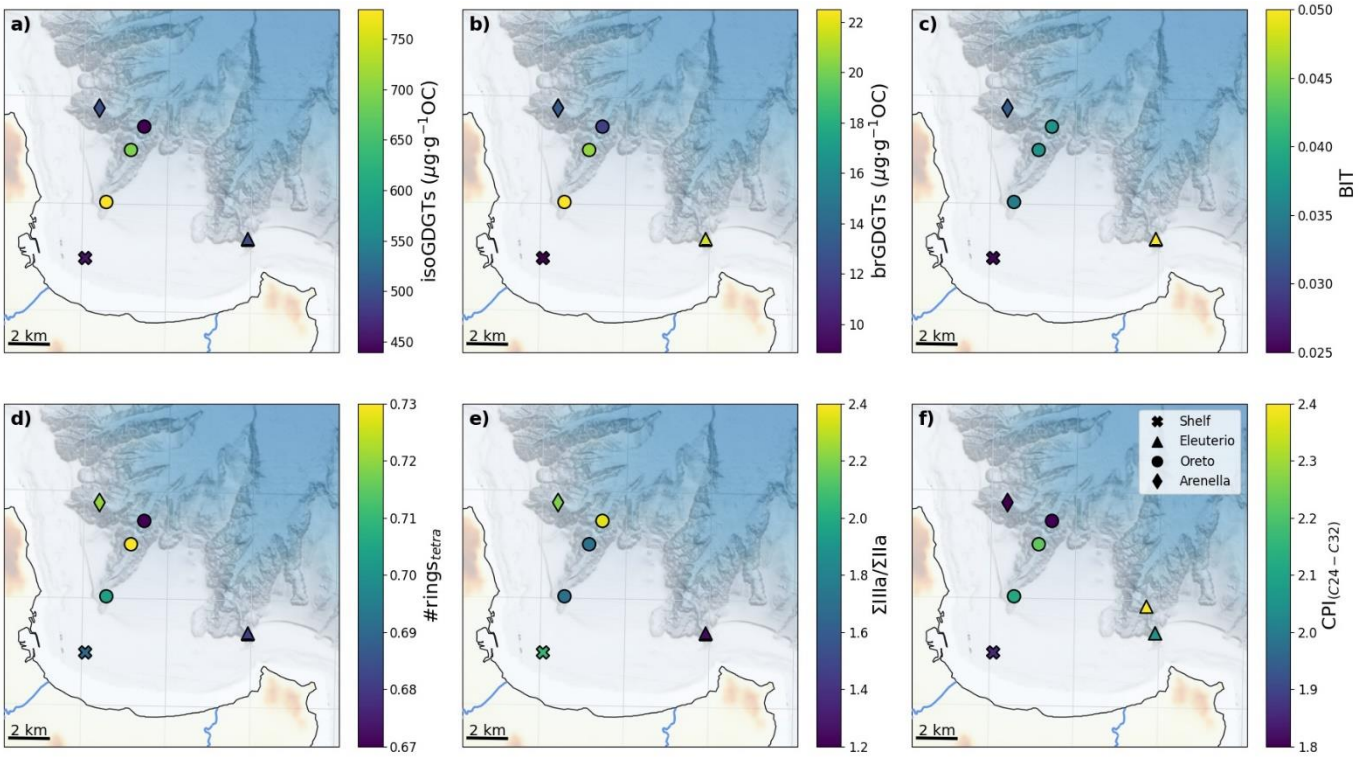

Figure S3. Spatial distribution of composition of GDGT proxies: a) isoGDGT concentrations, b) brGDGT concentrations, c) BIT index, d) #rings$_{tetra}$ ratio, e) ΣIIIa/ΣIIa ratio, and f) CPI$_{(C24-C32)}$ of HMW FA. Colour bars are adjusted to highlight the minimum, mean, and maximum values for each variable.

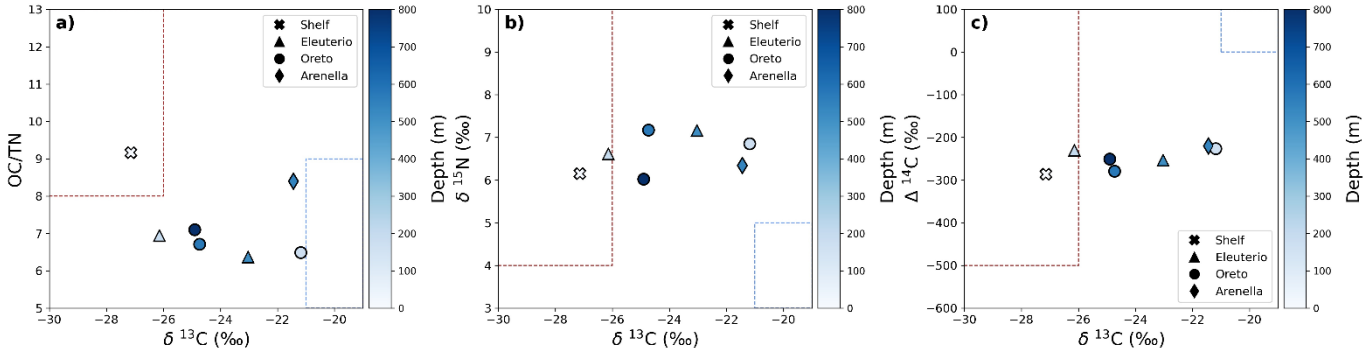

Figure S4. Scatter plots of OC/TN and δ^{13}C (a), δ^{15}N and δ^{13}C (b), Δ^{14}C and δ^{13}C (d) used for the two-dimension mixing models, showcasing the values of terrestrial (brown dashed lines) and marine (blue dashed lines) endmembers. See Table 1 for the values and sources of the different endmember values.

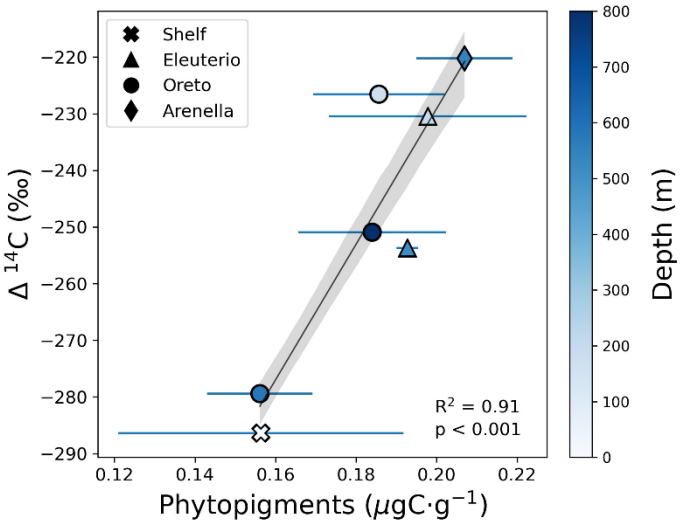

Figure S5. Relationship between phytopigment concentration and $\Delta^{14}C$, and fitting using a weighed-least squares regression, using the uncertainties from phytopigment concentrations as weights.

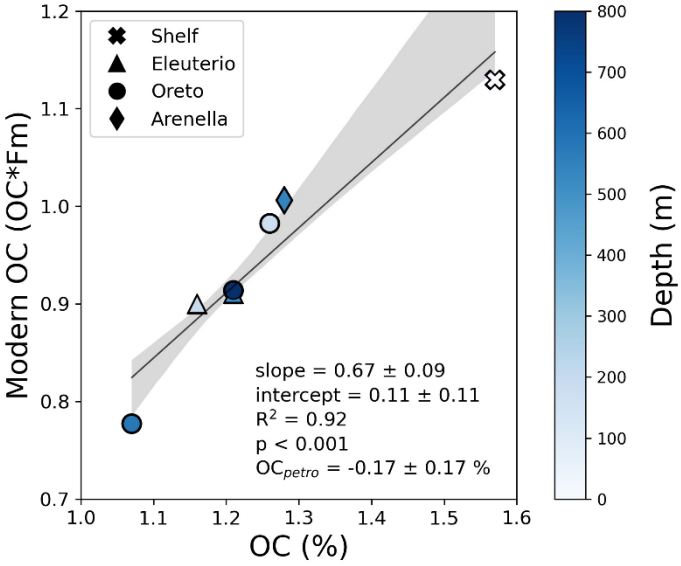

Figure S6. Relationship between modern OC (the product of OC content and radiocarbon fraction modern) and OC content. According to the fraction modern mixing model, the intercept of the fitting on the X-axis give the petrogenic OC content (Galy et al., 2008).

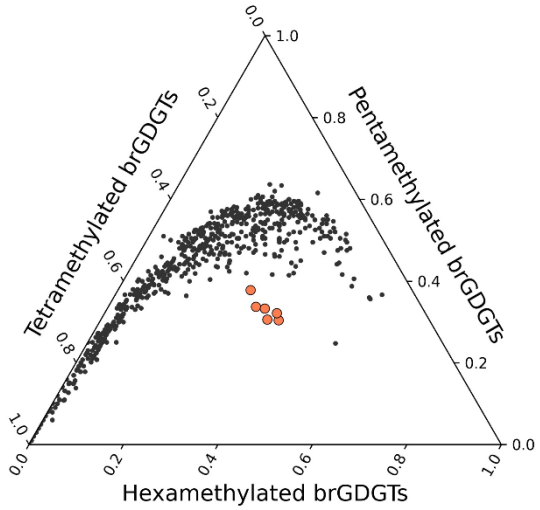

Figure S7. Ternary diagram showing the tetra-, penta-, and hexa-methylated brGDGTs in surface sediments of the Gulf of Palermo (pink circles) plotted together with the global soil and peat dataset (black dots) (Dearing Crampton-Flood et al., 2020). The clear offset of the Gulf of Palermo samples points to brGDGTs produced in-situ rather than being representative of soil-derived GDGTs.

References

Dearing Crampton-Flood, E., Tierney, J. E., Peterse, F., Kirkels, F. M. S. A. and Sinninghe Damsté, J. S.: BayMBT: A Bayesian calibration model for branched glycerol dialkyl glycerol tetraethers in soils and peats, Geochim. Cosmochim. Acta, 268, 142–159, doi:10.1016/j.gca.2019.09.043, 2020.

Galy, V., Beyssac, O., France-Lanord, C. and Eglinton, T.: Recycling of Graphite During Himalayan Erosion: A Geological Stabilization of Carbon in the Crust, Science (80-.)., 322(5903), 943–945, doi:10.1126/science.1161408, 2008.